Title

Isomerization and Fragmentation of Cyclohexanone in a Heated Micro-Reactor

Journal

The Journal of Physical Chemistry A, 119(51)

ISSN

1089-5639

Authors

Porterfield, Jessica P

Nguyen, Thanh Lam

Baraban, Joshua H

et al.

Publication Date

2015-12-24

DOI

10.1021/acs.jpca.5b10984

Peer reviewed

THE JOURNAL OF PHYSICAL CHEMISTRY A

Article

pubs.acs.org/JPCA

Isomerization and Fragmentation of Cyclohexanone in a Heated Micro-Reactor

Jessica P. Porterfield,[†] Thanh Lam Nguyen,[‡] Joshua H. Baraban,[†] Grant T. Buckingham,[†] Tyler P. Troy,[§] Oleg Kostko,[§] Musahid Ahmed,[§] John F. Stanton,[‡] John W. Daily,[∥] and G. Barney Ellison*[,†]

[†]Department of Chemistry and Biochemistry, University of Colorado, Boulder, Colorado 80309-0215, United States

[‡]Department of Chemistry, University of Texas at Austin, Austin, Texas 78712, United States

[§]Chemical Sciences Division, Lawrence Berkeley National Laboratories, Berkeley, California 94720, United States

[∥]Center for Combustion and Environmental Research, Department of Mechanical Engineering, University of Colorado, Boulder, Colorado 80309-0427, United States

Supporting Information

ABSTRACT: The thermal decomposition of cyclohexanone (C_6H_{10}═O) has been studied in a set of flash-pyrolysis microreactors. Decomposition of the ketone was observed when dilute samples of C_6H_{10}═O were heated to 1200 K in a continuous flow microreactor. Pyrolysis products were detected and identified by tunable VUV photoionization mass spectroscopy and by photoionization appearance thresholds. Complementary product identification was provided by matrix infrared absorption spectroscopy. Pyrolysis pressures were roughly 100 Torr, and contact times with the microreactors were roughly 100 μs. Thermal cracking of cyclohexanone appeared to result from a variety of competing pathways, all of which open roughly simultaneously. Isomerization of cyclohexanone to the enol, cyclohexen-1-ol (C_6H_9OH), is followed by retro-Diels–Alder cleavage to CH_2═CH_2 and CH_2═C(OH)–CH═CH_2. Further isomerization of CH_2═C(OH)–CH═CH_2 to methyl vinyl ketone (CH_3CO–CH═CH_2, MVK) was also observed. Photoionization spectra identified both enols, C_6H_9OH and CH_2═C(OH)–CH═CH_2, and the ionization threshold of C_6H_9OH was measured to be 8.2 ± 0.1 eV. Coupled cluster electronic structure calculations were used to establish the energetics of MVK. The heats of formation of MVK and its enol were calculated to be Δ_fH_{298}(*cis*-CH_3CO–CH═CH_2) = −26.1 ± 0.5 kcal mol^{-1} and Δ_fH_{298}(*s-cis*-1-CH_2═C(OH)–CH═CH_2) = −13.7 ± 0.5 kcal mol^{-1}. The reaction enthalpy $\Delta_{rxn}H_{298}$(C_6H_{10}═O → CH_2═CH_2 + *s-cis*-1-CH_2═C(OH)–CH═CH_2) is 53 ± 1 kcal mol^{-1} and $\Delta_{rxn}H_{298}$(C_6H_{10}═O → CH_2═CH_2 + *cis*-CH_3CO–CH═CH_2) is 41 ± 1 kcal mol^{-1}. At 1200 K, the products of cyclohexanone pyrolysis were found to be C_6H_9OH, CH_2═C(OH)–CH═CH_2, MVK, CH_2CHCH_2, CO, CH_2═C═O, CH_3, CH_2═C═CH_2, CH_2═CH–CH═CH_2, CH_2═$CHCH_2CH_3$, CH_2═CH_2, and HC≡CH.

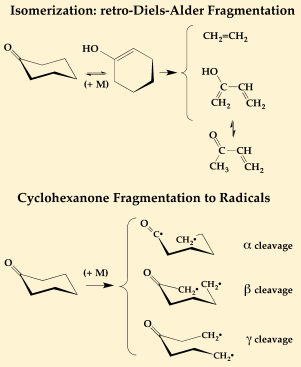

1. INTRODUCTION

Determining pathways for the decomposition of biofuels is the first step toward understanding more complex processes such as their combustion in an engine. It is important to identify the reactive intermediates and to establish the combustion mechanisms if biomaterials are to be adopted as fuels. Cyclohexanone, C_6H_{10}═O, a simple ketone, is one of the compounds under consideration as a second-generation biofuel.[1] Studies have shown that a diesel engine produces less soot when blends of cyclohexanone with synthetic Fischer–Tropsch fuels are used.[2] In separate studies, the sooting and chemiluminescence behaviors of bioderived and oxygenated fuels were studied in an optically accessible diesel engine.[1] From the combined soot and nitric oxide data, it was concluded that cyclic additives such as cyclohexanone are more efficient in soot abatement than others. The mechanisms by which cyclohexanone contributed to these results are poorly understood.

Only two experimental studies[3,4] and one modeling paper[5] have been dedicated to the pyrolysis or oxidation of cyclohexanone. A pioneering study[3] pyrolyzed cyclohexanone at 1300 K in ceramic tubes at pressures of 60 mTorr. Equation 1 shows the mole percent yield for each of the products detected[3] from the pyrolysis of cyclohexanone.

$$\begin{aligned} &C_6H_{10}{=}O\ (+M) \rightarrow CH_2{=}CH_2\ (52),\\ &CH_3CO{-}CH{=}CH_2\ (MVK)\ (15),\ CH_3CH{=}CH_2\ (10),\\ &CH_2{=}C{=}CH_2\ (4),\ CH_2{=}CHCH_2CH_3\ (4),\ HC{=}CH\ (3)\\ &,\ CH_3CH_3\ (2),\ CH_2{=}CH{-}CH{=}CH_2\ (2),\\ &\text{cyclopentane}\ (2),\ CH_2{=}CH{-}CH_2{-}CH{=}CH_2\ (2),\\ &\text{cyclopentadiene}\ (1),\ CH_2{=}CH{-}CHO\ (1),\ C_6H_6\ (1) \end{aligned} \quad (1)$$

The three most abundant pyrolysis products were ethylene, methyl vinyl ketone (MVK), and propene.

The kinetics of the oxidation of cyclohexanone in a jet-stirred reactor have also been reported.[4] Samples of cyclohexanone

Received: November 9, 2015
Revised: November 27, 2015
Published: November 30, 2015

DOI: 10.1021/acs.jpca.5b10984
J. Phys. Chem. A 2015, 119, 12635−12647

(1000−1500 ppm) in oxygen/nitrogen gas mixtures at 10 atm were heated to temperatures of 530−1220 K. After a fixed residence time of 0.7 s, the resulting products were sampled and identified by both infrared (IR) and gas chromatographic analysis. Unlike the previous pyrolysis experiments,[3] MVK was never found to be an important product in these oxidation experiments, even under the richest fuel conditions.

1.1. Plausible Decomposition Pathways. One could anticipate[3] that the pyrolysis of cyclohexanone might begin with the isomerization to the enol, C_6H_9OH, followed by a retro-Diels−Alder fragmentation. Alternatively, simple cleavage of C−C bonds within C_6H_{10}═O could result in the formation of three different sets of diradicals. These two potential pathways are shown in Scheme 1. The initial diradical products will be unstable; the fate of these radical species is explored in Scheme 2.

Scheme 1. Possible Pathways for Cyclohexanone Pyrolysis[a]

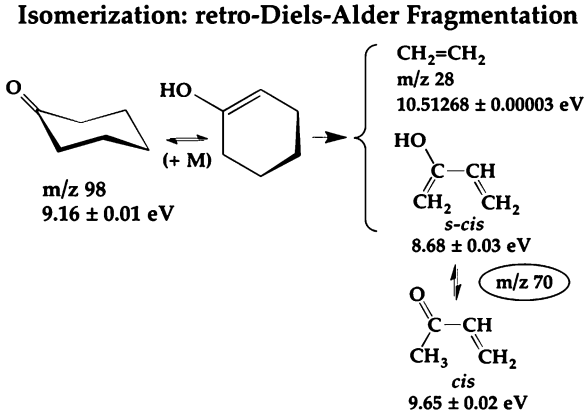

[a]Some species are identified by mass and ionization energy.

Thermodynamic quantities pertinent to the decomposition of cyclohexanone are summarized in Table 1. Enols such as C_6H_9OH and CH_2═C(OH)−CH═CH_2 in the retro Diels−Alder reaction are typically about 10 kcal mol^{-1} less stable than their corresponding ketones, cyclohexanone, and MVK. Common conjectures[5−9] for the barriers of the gas-phase keto/enol tautomerizations (>CH−CO− → >CH═C(OH)−) are approximately 65 kcal mol^{-1}. To estimate the thermochemistry for the cracking of C_6H_9−OH, we consider a similar alkene, cyclohexene. Cyclohexene has been observed[10] to fragment via retro Diels−Alder reaction: The $\Delta_{rxn}H_{298}$(cyclohexene → CH_2═CH_2 + CH_2═CH−CH═CH_2) is 40.0 ± 0.3 kcal mol^{-1} and the activation energy E_a is 62 kcal mol^{-1} (see entry 11 in Table 1). Consequently the threshold for cyclohexanone pyrolysis to ethylene and CH_2═C(OH)−CH═CH_2 is estimated to be roughly 75 kcal mol^{-1}. We also expect that the

Scheme 2. Decomposition of Cyclohexanone via α, β, and γ Cleavage[a]

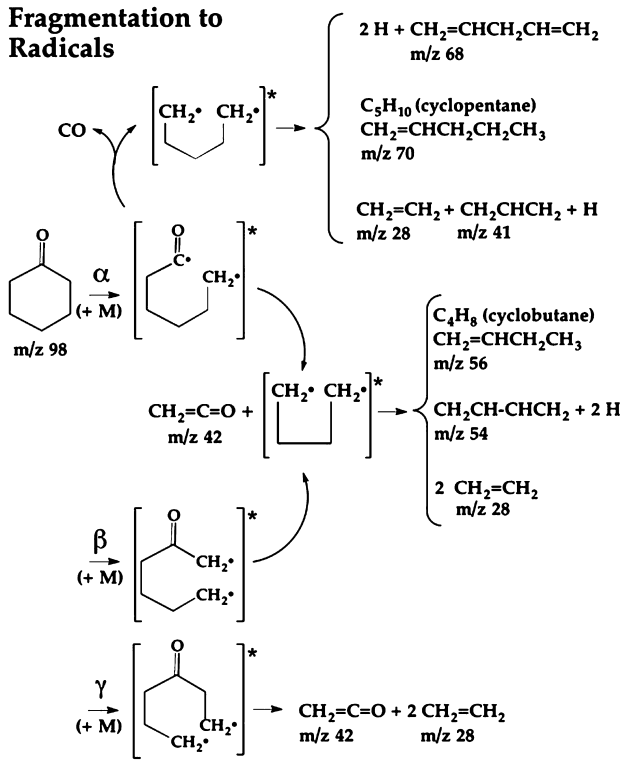

[a]Some species are identified by mass.

resulting CH_2═C(OH)−CH═CH_2 will subsequently isomerize to methyl vinyl ketone (MVK), CH_3CO−CH═CH_2.

The thermochemistry of the ring fragmentation at the bottom of Scheme 1 is difficult to assess. The energetics for the rupture of the ring are complicated because the diradical products are floppy molecules and the radical sites can be singlet or triplet coupled. We can estimate the bond energetics for the three different cleavage sites from the model compounds listed in Table 1: CH_3CHO, CH_3COCH_3, and $CH_3COCH_2CH_3$. The bond energies of the α C−H bonds of cyclohexanone are expected to be roughly 94 kcal mol^{-1} (entry 1 in Table 1), while the three C−C bonds of the ring (α, β, γ) are likely to be roughly 84 kcal mol^{-1} (entries 2−6 in Table 1). Applying these estimates to the pathways in Scheme 1, we anticipate cyclohexanone will initially isomerize and decompose to CH_2═CH_2 and CH_2═C(OH)−CH═CH_2. At slightly higher reactor temperatures, fragmentation of the cyclohexanone ring to diradicals should ensue.

The likely fates of the radicals at the bottom of Scheme 1 are explored in Scheme 2. Fragmentation of the cyclohexanone α C−C bond produces the unstable diradical, [•$CH_2CH_2CH_2CH_2CH_2CO$•]. This species can either decompose to CH_2═C═O and the [•$CH_2CH_2CH_2CH_2$•] diradical or shed carbon monoxide to produce the pentamethylene diradical, [•$CH_2CH_2CH_2CH_2CH_2$•]. The pentamethylene diradical can proceed to react in several ways. It can lose two H atoms via β-scission to produce CH_2═CH−CH_2−CH═CH_2 or ring close to produce cyclopentane. Pentamethylene could also internally disproportionate to CH_2═CH−$CH_2CH_2CH_3$ or extrude ethylene to form the trimethylene diradical [•$CH_2CH_2CH_2$•]. At the high temperatures of the microreactor, trimethylene diradical is expected to lose an H atom to produce

DOI: 10.1021/acs.jpca.5b10984
J. Phys. Chem. A 2015, 119, 12635−12647

Table 1. Thermochemistry of Cyclohexanone and Related Species

		(kcal mol^{-1})	ref
1	$DH_{298}(CH_3COCH_2-H)$	96 ± 2	34, 35
2	$DH_{298}(CH_3CO-CH_3)$	84.5 ± 0.5	36, 37
3	$DH_{298}(CH_3COCH_2-CH_3)$	84 ± 2	36, 37
4	$DH_{298}(CH_3CO-CH_2CH_3)$	83.6 ± 0.6	36, 37
5	$DH_{298}(CH_3-CH_2CH_3)$	89.1 ± 0.4	36, 37
6	$DH_{298}(CH_3CH_2-CH_2CH_3)$	88.0 ± 0.6	36, 37
7	$DH_{298}(CH_2CH-CH_2CH_3)$	100.0 ± 0.8	36, 37
8	$DH_{298}(CH_2CHCH_2-CH_3)$	76.4 ± 0.5	36, 37
9	$DH_{298}(CH_2CHCH_2-CHCH_2)$	87.3 ± 0.8	36, 37
10	$\Delta_{rxn}H_{298}(CH_2CHCH_2 \rightarrow H + CH_2{=}C{=}CH_2)$	56.2 ± 0.5	36, 37
11	$\Delta_{rxn}H_{298}(\text{cyclohexene} \rightarrow CH_2{=}CH-CH{=}CH_2 + CH_2{=}CH_2)$	40.0 ± 0.3	36
12	$\Delta_{rxn}H_{298}(s\text{-}cis\text{-}CH_2{=}C(OH)\text{-}CH{=}CH_2 \rightarrow s\text{-}cis\text{-}CH_3{-}CO{-}CH{=}CH_2)$	−12 ± 1	this work
13	$\Delta_{rxn}H_{298}(\text{cyclohexanone} \rightarrow CH_2{=}C(OH){-}CH{=}CH_2 + CH_2{=}CH_2)$	53 ± 1	this work[36]
14	$\Delta_{rxn}H_{298}(\text{cyclohexanone} \rightarrow CH_3{-}CO{-}CH{=}CH_2 + CH_2{=}CH_2)$	41 ± 1	this work[36]
15	$\Delta_{rxn}H_{298}(cis\text{-}CH_3{-}CO{-}CH{=}CH_2 \rightarrow CH_3CO + CH{=}CH_2)$	95 ± 1	this work[37]

the allyl radical, CH_2CHCH_2. Cleavage of either the α or β C−C bonds, followed by the loss of $CH_2{=}C{=}O$ in Scheme 2, leads to the formation of the tetramethylene diradical, [•$CH_2CH_2CH_2CH_2$•]. By analogy to the pentamethylene diradical, the tetramethylene diradical could decompose in four ways. The tetramethylene diradical could eliminate two H atoms to produce $CH_2{=}CH{-}CH{=}CH_2$ or ring close to produce cyclobutane. It could also internally disproportionate to $CH_2{=}CH{-}CH_2CH_3$ or collapse into two alkenes, $CH_2{=}CH_2$. Cleavage of the γ C−C bond in cyclohexanone in Scheme 2 yields a diradical that is anticipated to undergo β-scission to $CH_2{=}C{=}O$ and $CH_2{=}CH_2$.

1.2. Secondary Decompositions. Many of the initial products presented in Schemes 1 and 2 are expected to decompose further in the hot microreactor. Scheme 3 shows the likely fate of these primary products. At the top of Scheme 3, the pyrolysis of MVK is depicted. Initial loss of H atom results in the formation of ketene $CH_2{=}C{=}O$ and vinyl radical CH_2CH. Similarly, loss of CH_3 and CO also leads to the formation of vinyl radical. The vinyl radical will quickly fragment into acetylene and H atom in the hot microreactor.

The products of α and β-fragmentation are not stable and are not expected to survive in the hot microreactor. Decomposition of 1,4-pentadiene could produce $CH_2{=}CH{-}CH{-}CH{=}CH_2$ or CH_2CHCH_2 and vinyl radical. Cyclopentane and 1-pentene are expected to fragment to the allyl (CH_2CHCH_2) and ethyl (CH_2CH_3) radicals and ultimately to ethylene. Similarly, cyclobutane and 1-butene could crack apart to allyl and methyl radicals. At higher temperatures, the allyl radical is likely to further decompose by loss of an H atom to form allene, $CH_2{=}C{=}CH_2$.

Scheme 3. Decomposition of Primary Pyrolysis Products of Cyclohexanone

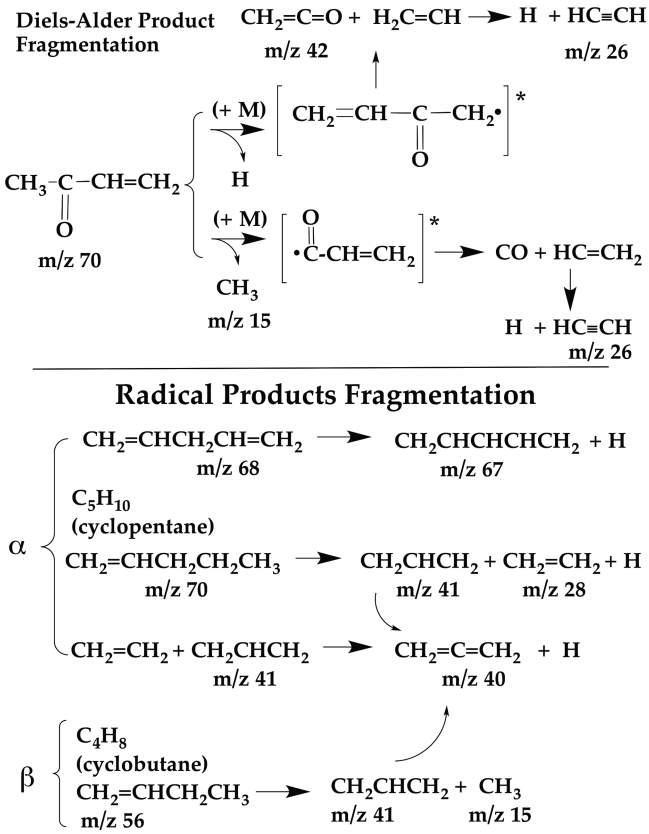

2. EXPERIMENTAL SECTION

2.1. Micro-Reactor. For this study of cyclohexanone, we have used several slightly different reactors, all of which have been described in detail.[11−14] At the Chemical Dynamics Beamline 9.0.2 of the Advanced Light Source (ALS) at Lawrence Berkeley National Laboratory (LBNL), we have deployed a continuous flow reactor that uses He as a carrier gas while we use pulsed reactors in Colorado with both He and Ar as carrier gases. Table 2 describes the experimental configurations in the three microreactors used for this study. In brief, the microreactors are silicon carbide (SiC) tubes that are resistively heated to temperatures of up to 1800 K. They range from 0.6 to 1 mm in diameter and are 2 to 3 cm long. The heated portion of the microreactor is 1 to 1.5 cm long. Temperatures are monitored using a Type C thermocouple attached to the tube with 0.005 in. tantalum wire. The accuracy of the thermocouple is 1.0% from 270 to 2300 K (Omega Engineering). Typical residence times of target molecules are 25−150 μs.[12] Pressure behind the reactor is typically 100−200 Torr and is measured with a capacitance manometer. At the reactor exit, the molecular beam supersonically expands into a vacuum chamber held at about 10^{-6} Torr. As a result of this expansion, the rotational and vibrational temperatures of the pyrolysis products are cooled. In the

DOI: 10.1021/acs.jpca.5b10984
J. Phys. Chem. A 2015, 119, 12635−12647

Table 2. Summary of Experimental Conditions and Reactor Geometries

experiment	flow (gas)	reactor I.D. × heated length	ionization source	inlet pressure (torr)	outlet pressure (torr)
PIMS at LBNL	continuous (He)	0.6 mm × 15 mm	synchrotron 7.4−30 eV	100−300	2×10^{-4}
PIMS in Colorado	pulsed (He)	1 mm × 15 mm	Nd:YAG 9th harmonic	1500	2×10^{-6}
FTIR in Colorado	pulsed (Ar)	1 mm × 10 mm	none	600−800	2×10^{-6}

Table 3. Ionization Energies of Important Organics

m/z	species	name	IE/eV	refs
1	H	H atom	13.59844 ± 0.00001	38
15	CH_3	methyl	9.8380 ± 0.0004	39
26	HC≡CH	acetylene	11.40059 ± 0.00001	40
28	CO	carbon monoxide	14.0136 ± 0.0005	41
28	CH_2=CH_2	ethylene	10.5127 ± 0.0003	42
39	$HCCCH_2$	propargyl radical	8.6982 ± 0.0005	43
40	CH_2=C=CH_2	allene	9.688 ± 0.002	44
40	CH_3C≡CH	propyne	10.3674 ± 0.0001	45
41	CH_2CHCH_2	allyl radical	8.1315 ± 0.0003	46
42	CH_2=C=O	ketene	9.6191 ± 0.0004	47
42	CH_2=CH−CH_3	propene	9.7435 ± 0.0005	48
43	CH_3CO	acetyl	6.95 ± 0.02	49
44	CH_3CHO	acetylaldehyde	10.2295 ± 0.0007	50
44	CH_2=CH−OH	ethenol	9.33 ± 0.05	51
54	CH_2=CH−CH=CH_2	1, 3-butadiene	9.082 ± 0.004	52
56	$(CH_2)_4$	cyclobutane	9.6 ± 0.1	53
56	CH_2=$CHCH_2CH_3$	1-butene	9.63 ± 0.02	53
56	*trans*-CH_3CH=$CHCH_3$	*trans*-2-butene	9.1259 ± 0.0005	48
70	CH_3CO−CH=CH_2	MVK	9.65 ± 0.05	54
70	CH_2=C(OH)−CH=CH_2	2-hydroxy-butadiene	8.68 ± 0.03	55
70	CH_2=$CHCH_2CH_2CH_3$	1-pentene	9.52 ± 0.02	53
70	C_5H_{10}	cyclopentane	10.3 ± 0.1	53
68	CH_2=CH−CH=CH−CH_3	1,2-pentadiene	8.61 ± 0.02	53
68	CH_2=$CHCH_2$CH=CH_2	1,4-pentadiene	9.62 ± 0.02	53
98	C_6H_{10}=O	cyclohexanone	9.16 ± 0.01	28
98	C_6H_9OH	cyclohexen-ol	≤8.2 ± 0.1	this work

expansion there are very few molecular collisions and chemistry effectively ceases.

Pyrolysis products exiting the SiC microreactor are detected and identified by a combination of photoionization mass spectroscopy (PIMS) and matrix-isolated infrared absorption spectroscopy (IR). In other studies, resonance-enhanced multiphoton ionization[15,16] (REMPI) and chirped-pulsed microwave spectroscopy[17,18] (CP-FTMW) have been used for product detection and identification. This combination of molecular diagnostics permits the detection of all of the pyrolysis products: atoms, organic radicals, and metastables.

2.2. Photoionization Mass Spectrometry. Photoionization mass spectrometry experiments were carried out in Colorado and at the Chemical Dynamics Beamline 9.0.2 of the LBNL's ALS. These experiments were conducted with concentrations of 0.008 to 0.06% cyclohexanone in He (cyclohexanone-d_0 99.8% and cyclohexanone-2,2,6,6-d_4 98%; Aldrich). Experiments in Colorado employ a pulsed gas flow with a pulsed VUV laser. The gas mixture is pulsed into the reactor using a Parker General valve fired at 10 Hz. Backing pressures are typically 1500 Torr. Roughly 1 cm from the exit of the reactor, the molecular beam is skimmed through a 2 mm aperture and continues to flow downstream toward the ionization region. The ionization source is the ninth harmonic of a Nd:YAG laser (118.2 nm, 10 Hz). The Nd:YAG third harmonic is directed into a tripling cell containing 150 Torr of a 10:1 Ar/Xe mixture where 118.2 nm (10.487 eV) light is generated. This beam is focused using a MgF_2 lens into the ionization region where it encounters the skimmed molecular beam. Dual-stage ion optics extract the resulting cations into a Jordan reflectron time-of-flight mass spectrometer with chevron microchannel plate detectors.[14,19,20] PIMS spectra are a composite of 1000 scans with a minimum mass resolution $m/\Delta m$ of 400. Calibration is carried out before and after scanning to ensure that no drifting occurs during data collection.

PIMS experiments at the ALS are conducted using synchrotron radiation as the ionization source. The quasi-continuous (500 MHz) radiation can be tuned between 7.4 to 19 eV. Gas flow to the reactor is held at a continuous volumetric flow rate of 260 sccm (standard cm^3 min^{-1}) using an MKS P4B (0−200 sccm N_2) mass flow controller. Backing pressures are roughly 100 Torr at room temperature and up to 300 Torr at 1600 K. Continuous flow and the high repetition rate increase the PIMS signals by more than two orders of magnitude compared with the pulsed microreactor in Colorado. Typical photon fluxes are roughly 10^{13} photons per second.[11] The start time for the ion packet in the TOF spectrometer is provided by pulsing the repeller plate of the ion optics. Photoionization efficiency curves are normalized by dividing the ion count by the photocurrent at each photon energy.

2.3. Matrix Isolation Infrared Spectroscopy. To collect IR spectra of the initial reactive products of thermal

DOI: 10.1021/acs.jpca.5b10984
J. Phys. Chem. A 2015, 119, 12635−12647

Table 4. Calculated Heat of Formation (kcal mol^{-1}) of Methyl Vinyl Ketone and the *s-trans*-1-Enol from Isodesmic Reactions

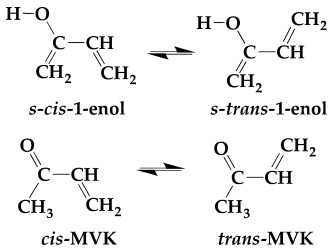

working reactions	$\Delta_{rx}H_0$	Δ_fH_0
trans-MVK + H_2 → CH_3CHO + C_2H_4	−0.13	−22.29
trans-MVK + CH_4 → CH_3CHO + C_3H_6	4.68	−21.82
trans-MVK + CH_4 → $CH_3C(O)CH_3$ + C_2H_4	9.52	−22.18
trans-MVK + C_2H_6 → $CH_3C(O)CH_3$ + C_3H_6	−0.96	−21.96
s-trans-1-enol + CH_4 → CH_2=CH(OH) + C_3H_6	9.76	−12.26
s-trans-1-enol + CH_4 → CH_3OH + CH_2=CH−CH=CH_2	13.15	−12.37
average Δ_fH of *trans*-MVK, *trans*-CH_3−CO−CH=CH_2		−22.30 ± 0.24
average Δ_fH of *cis*-MVK, *cis*-CH_3−CO−CH=CH_2		−22.43 ± 0.24
average Δ_fH of *s-trans*-1-enol, *trans*-CH_2=C(OH)−CH=CH_2		−12.32 ± 0.24

decomposition, we employ the technique of matrix isolation; this experiment has previously been described.[11,13] In brief, gas mixtures (0.25% cyclohexanone in argon) are pulsed (Parker General Valve) into the hot microreactor at 10 Hz. Products from the microreactor are directed toward a cold CsI window where they are frozen into an argon matrix and subsequently analyzed by IR absorption spectroscopy. The CsI window is held at 20 K by a dual-stage He cryostat (HC-2 APD Cryogenics). Infrared absorption spectra are collected with a commercial FT-IR (Nicolet 6700) fixed with an MCT-A detector (4000−650 cm^{-1}) and IR spectra are averaged over 500 scans with 0.25 cm^{-1} step sizes.

3. RESULTS

3.1. Theoretical Thermochemistry. The heats of formation of many of the species in Schemes 1−3 are available (Table 1). Surprisingly, the heat of formation of CH_3CO−CH=CH_2 has not been measured; this is a very important compound in atmospheric chemistry and combustion processes. We have computed heats of formation of MVK and its enol isomer using a medium accuracy extrapolated ab initio thermochemistry protocol, which is a modification of the HEAT method.[21−23] This approach has been used in a recent paper[24] and is briefly described in the Supporting Information. The modified HEAT procedure is intended for medium-sized molecular systems and achieves a thermochemical accuracy of ~0.5 kcal mol^{-1} (see Table S1 in the Supporting Information). Further tests for a set of molecules used in the HEAT protocol are in progress to validate the performance of this procedure and will be reported in due course.

In this work, heats of formation of MVK and its enol are computed using isodesmic reactions that are expected to give better results than those derived simply from total atomization energies, owing to cancellation of systematic errors. Heats of formation at 0 K (Table 4) are found to be Δ_fH_0(*cis*-CH_3COCH=CH_2) = −22.5 ± 0.5 kcal mol^{-1} and Δ_fH_0(*s-cis*-1-CH_2=C(OH)−CH=CH_2) = −9.8 ± 0.5 kcal mol^{-1}. Note that we are able to characterize four distinct enol conformers. With the thermochemical values at 0 K in hand, heats of formation under the standard conditions (298 K and 1 atm) are then computed using[25] eq 2

$$\Delta_fH_{298}(\mathrm{M}) = \Delta_fH_0(\mathrm{M}) + (H_{298} - H_0)(\mathrm{M}) - \sum N_{\mathrm{Ai}}(H_{298} - H_0)_{\mathrm{Ai}} \quad (2)$$

Here M denotes either MVK or enol, A_i represents an H, C, or O atom, and N_{Ai} is the number of A_i atoms in the molecule. $H_{298} - H_0$ is the thermal correction to the enthalpy, computed using the partition functions for vibrations, rotations, and translations in the anharmonic oscillator (in the VPT2 approximation[26]) and rigid-rotor approximation.[27] The heats of formation at 0 and 298 K are Δ_fH_0(M) and Δ_fH_{298}(M). Table 5 shows the heat of formation obtained at 298 K to be −26.1 ± 0.5 kcal mol^{-1} for *cis*-MVK and −13.7 ± 0.5 kcal mol^{-1} for its enol form, *s-cis*-1-CH_2=C(OH)−CH=CH_2. In addition, the effects of two hindered internal rotations (HIRs) in *cis*-MVK are also investigated. HIRs affect zero-point vibrational energies and thermal corrections and therefore can influence thermochemistry. The effects of two HIRs in cis-MVK are moderate; they shift heats of formation by <0.1 kcal mol^{-1} (see Table 5). It should be mentioned that when the hindered internal rotors are involved, heats of formation of MVK include contributions of both cis and trans conformers of MVK because the potential surface for hindered internal rotors contains both conformers.

Table 5. Calculated Thermal Correction Energies (kcal mol^{-1}) and Heats of Formation (kcal mol^{-1}) of MVK at 298 K

species	Δ_fH_0	$H_{298} - H_0$	Δ_fH_{298}
cis-MVK	−22.4 ± 0.5	4.363	−26.2 ± 0.5
	−22.5 ± 0.5[a]	4.553[a]	−26.1 ± 0.5[a]
trans-MVK	−22.3 ± 0.5	4.382	−25.8 ± 0.5
s-trans-1-enol	−12.3 ± 0.5	4.135	−16.3 ± 0.5
s-cis-1-enol	−9.8 ± 0.5	4.145	−13.7 ± 0.5
H	51.633	1.01	52.103
C	170.025	0.25	171.336
O	58.997	1.037	59.567

[a]Two hindered internal rotors are assumed to be separable from the remaining vibrations, and each one is treated as a separated 1D-hindered internal rotor.

3.2. Photoionization. Photoionization mass spectroscopy is a convenient method to track the decomposition channels

DOI: 10.1021/acs.jpca.5b10984
J. Phys. Chem. A 2015, 119, 12635−12647

presented in Schemes 1 − 3. However, use of a fixed frequency VUV light source in PIMS can lead to problems with ion fragmentation. The ionization energy (IE) of cyclohexanone[28,29] is 9.2 eV (see Table 3), and preliminary PIMS spectra taken in Colorado employ a 118.2 nm laser (10.487 eV); see Figure 1.

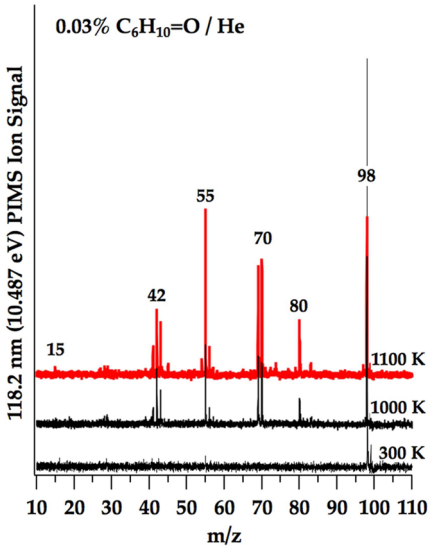

Figure 1. Photoionization mass spectrum from pulsed 118.2 nm PIMS. Mixture is 0.03% cyclohexanone in He heated up to 1100 K in a pulsed microreactor.

Ionization is 1.3 eV above the threshold for cyclohexanone and, consequently, the $[\text{cyclohexanone}]^+$ radical-cation is chemically activated and may fragment ("dissociative ionization").

$$C_6H_{10}{=}O + \hbar\omega_{118.2nm} \rightarrow [C_6H_{10}{=}O^*]^+(m/z\ 98) \rightarrow \text{daughter ions} \quad (3)$$

Figure 1 shows a normal mass spectrum at 300 K with only the parent species (m/z 98) present. No dissociative ionization is evident. Pyrolysis of cyclohexanone in the pulsed reactor starts at 1000 K as shown by the presence of MVK, m/z 70, and $CH_2{=}C{=}O$, m/z 42. Other prominent peaks are m/z 55, m/z 69, and m/z 80. We believe that these and other ions result from fragmentation of a mixture of the cyclohexanone radical cation, $[C_6H_{10}{=}O]^+$ and the enol cation, $[C_6H_9OH]^+$. A more detailed discussion of dissociative ionization is deferred until the end of the paper following the detection of the neutral enols, C_6H_9OH and $CH_2{=}C(OH){-}CH{=}CH_2$. To circumvent dissociative ionization, tunable synchrotron VUV radiation is used as the photoionization source.

3.3. Product Identification with Tunable VUV Radiation. PIMS with tunable VUV radiation is an effective means to avoid dissociative ionization. Use of VUV radiation just above the ionization threshold suppresses subsequent fragmentation of the parent ions. With synchrotron VUV radiation, photoionization mass spectrometry was used to observe the decomposition of dilute samples of cyclohexanone in He (0.03%) at 1200 K. To confirm the retro Diels−Alder mechanism (Scheme 1), we searched for the characteristic enols. Figure 2 is a PIMS spectrum taken under continuous flow conditions at the ALS; the radiation is tuned to 9.0 eV. The enol of MVK, $CH_2{=}C(OH){-}CH{=}CH_2$ (m/z 70), has a measured ionization energy of 8.7 eV (Table 3). Similarly, Table 3 shows the IE($CH_2{=}CHOH$) to be 1 eV below the IE(CH_3CHO). Thus, we might expect that the

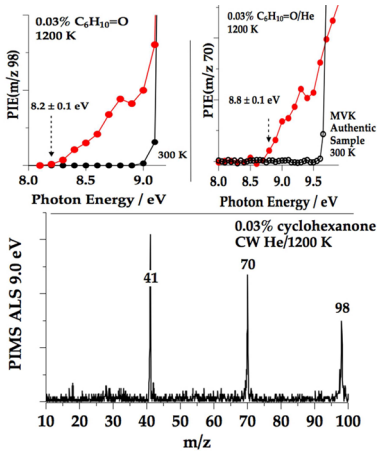

Figure 2. Photoionization mass spectrum (9.0 eV) of cyclohexanone in He heated to 1200 K in a continuous flow microreactor. The top insets show the PIE(m/z 98). The appearance energy of 8.2 ± 0.1 eV is an upper bound to $IE(C_6H_9{-}OH)$. The PIE(m/z 70) has an appearance energy of 8.8 ± 0.1 eV in agreement with that of $IE(CH_2{=}C(OH){-}CH{=}CH_2)$; see Table 3.

enol of cyclohexanone (C_6H_9OH, m/z 98) will ionize around 8.2 eV, roughly 1 eV lower than the parent ketone (Table 3). Photoionization efficiency curves (PIEs) of the ionization thresholds further confirm the identity of both enols at m/z 98 and m/z 70 by providing characteristic appearance energies. The top insets in Figure 2 show the PIE of m/z 98, and the appearance energy of 8.2 ± 0.1 eV is observed in the expected region. The PIE of m/z 70 at the top of Figure 2 displays an appearance energy of 8.8 ± 0.1 eV that is characteristic of $CH_2{=}C(OH){-}CH{=}CH_2$ (see Table 1). The two features in Figure 2 at m/z 98 and m/z 70 cannot be the ions $C_6H_{10}{=}O^+$ or $CH_3COCH{=}CH_2^+$ because 9.0 eV is significantly below their ionization thresholds. The m/z 98 and m/z 70 features are therefore assigned to the enols, $C_6H_9OH^+$ and $CH_2{=}C(OH){-}CH{=}CH_2^+$. The other product of the retro Diels−Alder reaction is ethylene. At 1200 K, a PIE of m/z 28 finds an appearance energy that is characteristic of $CH_2{=}CH_2$ at 10.5 eV (see Supplemental Figure S1). All of the Diels−Alder products in Scheme 1 have been identified when cyclohexanone is heated to 1200 K.

Evidence of the ring cleavage channels begins with an intense feature in Figure 2 at m/z 41, a signature of the allyl radical, CH_2CHCH_2. Allyl radicals originate from the (α and β) channels described in Schemes 2 and 3. The production of allyl radical from cyclohexanone is accompanied by ketene m/z 42. Figure 3 is a PIMS of cyclohexanone at 1200 K with the synchrotron tuned to 9.7 eV. A new feature at m/z 42 is now apparent and is assigned to be $CH_2{=}C{=}O$.

Figure 4 shows the result of 10.1 eV PIMS of cyclohexanone heated to 1200 K. Several new features appear at m/z 15, 40, 43, 54, 55, and 56. The inset at the top of Figure 4 shows the PIE scans for m/z 41 (CH_2CHCH_2) and m/z 42 ($CH_2{=}C{=}O$); the thresholds for both of these ions demonstrate the presence of allyl radical and ketene in the output of the microreactor (see Table 3). (The presence of both allyl radical and ketene are further confirmed by IR spectra, vide infra.) The ion at m/z 15 arises from the CH_3 radical. Whereas methyl is not present in Schemes 1 and 2, it is a predicted product of the pyrolysis of MVK; see Scheme 3. This scheme predicts thermal cracking of

DOI: 10.1021/acs.jpca.5b10984
J. Phys. Chem. A 2015, 119, 12635−12647

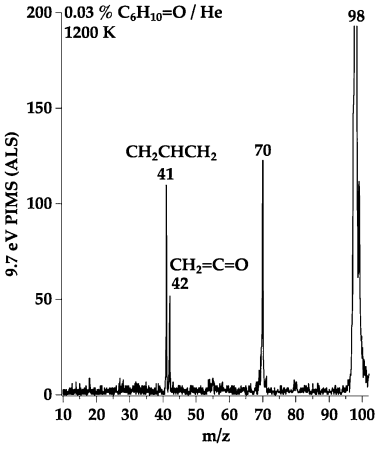

Figure 3. Photoionization mass spectrum at 9.7 eV of cyclohexanone at 1200 K in a continuous flow microreactor.

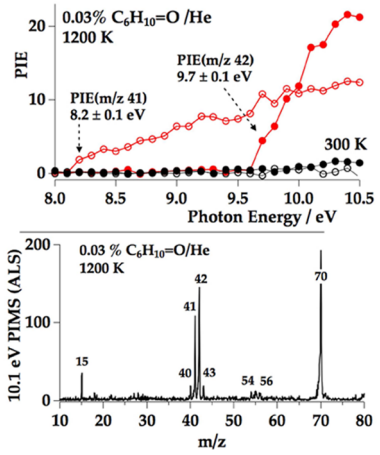

Figure 4. Photoionization mass spectra at 10.1 eV of cyclohexanone at 1200 K in a continuous flow microreactor. The inset at the top shows the PIE(m/z 41) and PIE(m/z 42); the thresholds for both of these ions confirm the presence of CH_2CHCH_2 and CH_2CO (see Table 3).

$CH_3CO-CH=CH_2$ to $CH_2=C=O$ and $HC\equiv CH$ in addition to methyl radical.

Because PIMS confirms the formation of $CH_2=C(OH)-CH=CH_2$ from cyclohexanone heated to 1200 K, the fate of both MVK and its enol must be discussed. Figure 5 shows 10.0 eV PIMS scans of the products arising from an authentic sample of $CH_3COCH=CH_2$. The IE(MVK) is 9.65 ± 0.05 eV (see Table 3); at 300 K, there is no dissociative ionization and only ions at m/z 70 are detected. Heating MVK to 1200 K produces faint signals at m/z 15, 18, and 55. As the temperature increases to 1500 K, ions at 15, 27, 42, and 55 are clearly present. Figure 6 shows scans of the PIE(m/z 70) resulting from heating MVK to 1100 and 1200 K. The threshold for PIE(m/z 70) at 1200 K is consistent with the presence of the enol, $CH_2=C(OH)-CH=CH_2$. Figure 7 shows scans of the photoionization efficiency curves for m/z 15, 26, and 42. The thermal cracking of an authentic sample of MVK at 1200 K would appear to confirm the chemistry in Scheme 3. The PIE(m/z 15), PIE(m/z 26), and PIE(m/z 42) traces all show the proper appearance energies for CH_3, $HC\equiv CH$, and $CH_2=C=O$. The species at m/z 27 ($CHCH_2^+$) and 55 (CH_2CHCO^+) are due to dissociative ionization from the MVK enol, while m/z 18 is background H_2O ionized by the higher synchrotron harmonics.

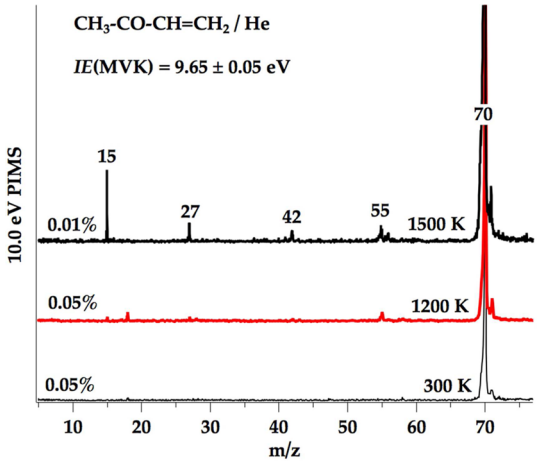

Figure 5. Photoionization mass spectra at 10.0 eV of an authentic sample of $CH_3COCH=CH_2$ (MVK) at room temperature, 1200 K, and 1300 K in a continuous flow SiC microreactor.

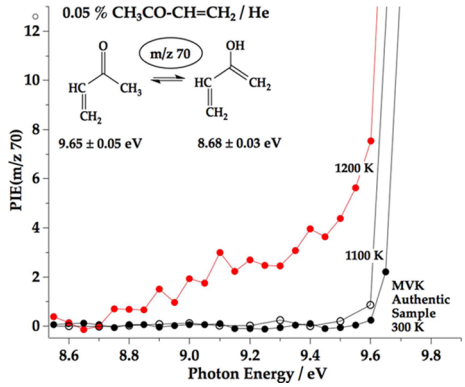

Figure 6. Photoionization efficiency curves for m/z 70 from an authentic sample of $CH_3COCH=CH_2$ (MVK) at room temperature, 1100 K, and 1200 K in a continuous flow SiC microreactor.

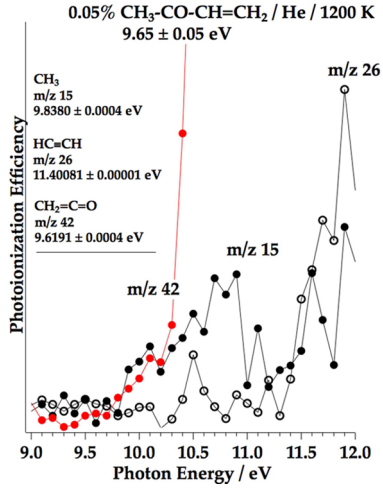

Figure 7. Photoionization efficiency scans at m/z 15, m/z 26, and m/z 42 from a dilute (0.05%) sample $CH_3COCH=CH_2$ (MVK)/He at 1200 K in a continuous flow SiC microreactor.

In the remainder of this subsection, having confirmed the presence of all possible channels shown in Schemes 1−3, we now discuss the rest of the predicted products and observed PIMS peaks. Other possible products in Figure 4 resulting from

DOI: 10.1021/acs.jpca.5b10984
J. Phys. Chem. A 2015, 119, 12635−12647

Scheme 2 are cyclopentane (m/z 70), 1,4-pentadiene (m/z 68), cyclobutane (m/z 56), 1-butene (m/z 56), and 1,3-butadiene (m/z 54). Cyclopentane will be masked because m/z 70 also belongs to the enol $CH_2{=}CH{-}C(OH){-}CH{=}CH_2$, which ionizes at 8.7 eV (see Table 3). The feature at m/z 56 in Figure 4 could be due to either cyclobutane or 1-butene; however, the PIE(m/z 56) is inconclusive. The presence of 1,3-butadiene (m/z 54) is confirmed by the PIE(m/z 54) scan with the proper appearance energy of 9.2 ± 0.2 eV (Figure S2). Other small features in Figure 4 are assigned to $CH_2{=}C{=}CH_2$ (m/z 40) and acetyl (m/z 43). Scheme 2 predicts the formation of allene from pyrolysis of allyl radical; the CH_3CO^+ ion is the product of dissociative ionization of the enol of MVK.

Diels–Alder fragmentation (Scheme 1) and all of the radical channels in Scheme 2 predict the formation of ethylene. The bottom panel of Figure 8 is a 10.7 eV PIMS scan of the

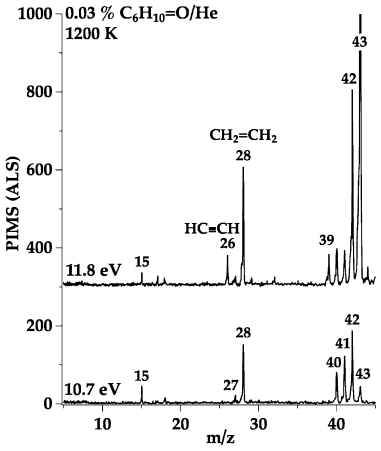

Figure 8. Photoionization mass spectrum (10.7 and 11.8 eV) of cyclohexanone heated to 1200 K in a continuous flow microreactor.

cyclohexanone pyrolysis products in a 1200 K continuous flow microreactor. The small feature at m/z 43 is CH_3CO^+ while that at m/z 27 is $HCCH_2^+$, and both arise from MVK dissociative ionization (Scheme S2). There is also a small feature at m/z 18 that is H_2O^+ resulting from ionization of background water by synchrotron higher harmonics. The top panel of Figure 8 is an 11.8 eV PIMS scan. In addition to the intense ethylene peak (m/z 28), a new feature is observed at m/z 26, which is attributed to HC≡CH. Additional evidence of this assignment is a PIE with the appropriate appearance energy of 11.4 ± 0.1 eV (see Figure S1). PIMS of heated cyclohexanone with 11.8 eV is accompanied by extensive dissociative ionization that is the source of the intense CH_3CO^+ feature at m/z 43. The feature at m/z 39 is $HCCCH_2^+$, and this is probably from dissociative ionization as well. The likely pathways for the formation of these daughter ions are shown in the Schemes S1 and S2 in the Supporting Information.

3.4. Matrix Infrared Absorption Spectroscopy. We now turn to IR spectroscopy to further confirm many of the photoionization assignments. Heating a dilute sample of cyclohexanone (0.25% in Ar) in a pulsed SiC microreactor to 1300 K leads to the pyrolysis of the ketone. Figure 9 is the argon matrix IR spectrum of some of the pyrolysis products. The presence of ethylene and MVK is observed, as expected from the retro Diels–Alder fragmentation. The intense $\nu_7(CH_2{=}CH_2)$ is detected; the characteristic >C=O stretch of MVK, $\nu_6(CH_3C(=O)CHCH_2)$, as well as ν_{23}(MVK) is also shown.

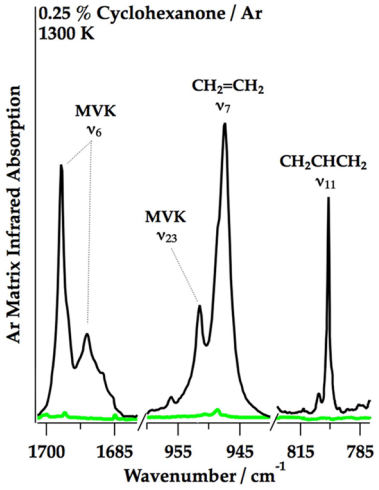

Figure 9. Infrared spectrum of cyclohexanone (0.025%) at 1300 K in a pulsed flow microreactor. Features for ethylene,[30] $\nu_7(CH_2{=}CH_2)$, methyl vinyl ketone,[56] ν_6(MVK), and allyl radical,[57] $\nu_{11}(CH_2CHCH_2)$, are assigned. Green trace is Ar background heated to 1300 K.

As in the 9.0 eV PIMS Figure 2, IR signals from the allyl radical appear in tandem with the retro Diels–Alder products, signifying that all channels presented in Scheme 1 are active under the same reaction conditions. Figure 10 confirms the production of

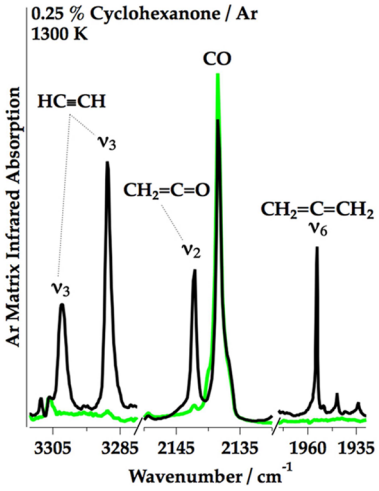

Figure 10. Argon matrix IR spectrum of cyclohexanone at 1300 K in a pulsed flow microreactor. Bands for acetylene,[30] ν_3(HCCH), ketene,[58] $\nu_2(CH_2{=}C{=}O)$, and allene,[30] $\nu_6(CH_2{=}C{=}CH_2)$, are assigned. The green trace is Ar background heated to 1300 K.

acetylene, ketene, and allene: ν_3(HC≡CH), $\nu_2(CH_2{=}C{=}O)$, and $\nu_6(CH_2{=}C{=}CH_2)$ are all observed. Acetylene arises from the further decomposition of MVK (Scheme 3). The ν_6 band for allene in Figure 8 is the >C=C=C< asymmetric stretch and is characteristic of cumulated double bonds.[30] The IR spectra confirms the PIMS assignment of $CH_2{=}C{=}CH_2$ (m/z 40) in Figure 4. Although most products in the infrared spectra presented here (Figures 9 and 10) display only one distinctive vibrational band of a species, in all cases many other IR bands were confirmed as well.

3.5. H-Atom Catalysis. As previously mentioned, the experiments (Figure 2) provide strong evidence of the production of the enols of cyclohexanone and MVK. A potential complication is that these isomers may not be produced by

DOI: 10.1021/acs.jpca.5b10984
J. Phys. Chem. A 2015, 119, 12635–12647

Scheme 4. Predicted Cyclohexanone d_0 and d_4 H/D Atom Chemistry with H Catalysis

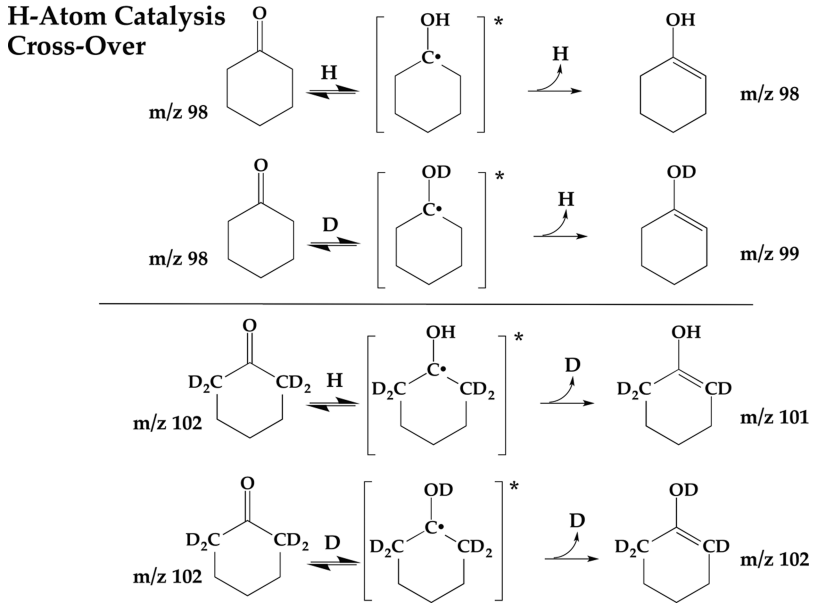

unimolecular processes but are the result of H-atom chemistry. The detection of ketene and allyl radicals as pyrolysis products provides strong evidence of the radical channels in Scheme 2. The formation of CH_2CHCH_2 radicals in Scheme 2 is accompanied by the production of H atoms; consequently, there may be many reactive hydrogen atoms present in the hot microreactor. If the cyclohexanone samples undergoing pyrolysis are not dilute enough, there is the possibility that H atoms could catalyze the keto/enol isomerization

$$C_6H_{10}{=}O + H \leftrightharpoons [C_6H_{10}{-}OH]^* \rightarrow C_6H_9OH + H \quad (4)$$

The pyrolysis of a 50:50 mixture of cyclohexanone-d_0 and cyclohexanone-d_4, however, would reveal the presence of hydrogen atom catalysis as described by eq 4. This crossover experiment is outlined in Scheme 4. H-atom catalysis in 50:50 mixture of cyclohexanone-d_0 (m/z 98) and cyclohexanone-d_4 (m/z 102) would lead to a mixture of isotopomers at m/z (98, 99, 101,102).

Figure 11 shows the experimental result of the thermal cracking of a dilute mixture (0.06% in helium) of a 50:50 mixture of cyclohexanone-d_0 and cyclohexanone-d_4. In this experiment, the cyclohexanone pyrolysis is carried out in a pulsed SiC microreactor with 118.2 nm (10.487 eV) PIMS detection. The PIMS scan at 300 K shows only peaks at m/z 98 and m/z 102. Heating to 1200 K, where keto/enol isomerization is thought to occur, does not produce any signals at m/z 99 or m/z 101. Consequently, there is no evidence produced for H atom catalysis in the decomposition of cyclohexanone in our reactor at concentrations <0.06%, and it therefore seems that secondary chemistry of this kind is not occurring under the reaction conditions used in our experiments.

4. DISCUSSION

Pyrolysis of cyclohexanone in a continuous, heated microreactor leads to decomposition of the ketone at a reactor temperature of 1200 K. All of the PIMS, PIE, and IR spectra lead to the conclusion that cyclohexanone thermally fragments by the multiple pathways depicted in Schemes 1−3. Care has been taken to use dilute cyclohexanone samples to avoid bimolecular

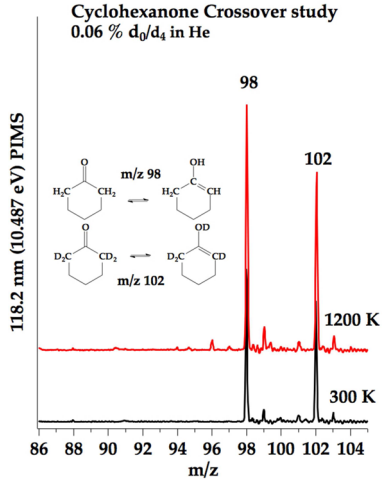

Figure 11. Photoionization mass spectrum of cyclohexanone d_0/d_4 crossover experiment at 118.2 nm (10.487 eV) in a pulsed microreactor. The feature at m/z 99 is the ^{13}C isotope peak of $C_6H_{10}{=}O$ and m/z 101 is a contamination of cyclohexanone d_4 sample.

chemistry as explicitly discussed toward the end of the previous section. A summary of all of the results for the pyrolysis of cyclohexanone is in Table 6. Many of the predicted products from Schemes 1−3 have been detected by at least two complementary measurements.

Both the retro-Diels−Alder fragmentation (Scheme 1) and the radical decomposition channels open simultaneously near 1200 K, as demonstrated by the 9.0 eV PIMS spectra in Figure 2. The presence of the two enols, cyclohexen-1-ol (C_6H_9OH) and 1,3 butadien-2-ol ($CH_2{=}C(OH){-}CH{=}CH_2$), is a signature for the keto/enol isomerization attendant to the retro-Diels−Alder fragmentation. Allyl radical (CH_2CHCH_2) arises from radical cleavage only and is detected simultaneously with ketene ($CH_2{=}C{=}O$).

At 1200 K, it is evident that some of primary cyclohexanone pyrolysis products are further decomposing. The PIE scan in Figure 7 confirms that MVK decomposes to produce small amounts of CH_3, $CH_2{=}C{=}O$, and $HC{\equiv}CH$. The 118.2 nm

DOI: 10.1021/acs.jpca.5b10984
J. Phys. Chem. A 2015, 119, 12635−12647

Table 6. Detected Products from 1200 K Pyrolysis of Cyclohexanone

m/z	species	name	PIMS	PIE	IR
15	CH_3	methyl radical	Figure 4	Figure 5	
26	$HC{\equiv}CH$	acetylene	Figure 6	Figure S1	Figure 8
28	$CH_2{=}CH_2$	ethylene	Figure 6	Figure S1	Figure 7
40	$CH_2{=}C{=}CH_2$	allene	Figure 4		Figure 8
41	CH_2CHCH_2	allyl radical	Figure 2	Figure 4	Figure 7
42	$CH_2{=}C{=}O$	ketene	Figure 3	Figure 4	Figure 8
54	$CH_2{=}CH{-}CH{=}CH_2$	1,3-butadiene	Figure 4	Figure S2	
56	$CH_2{=}CHCH_2CH_3$	1-butene	Figure 4		
56	C_4H_8	cyclobutane			
68	$CH_2{=}CHCH_2CH{=}CH_2$	1,4-pentadiene			
70	$CH_2{=}CHCH_2CH_2CH_3$	1-pentene			
70	C_5H_{10}	cyclopentane			
70	$CH_3CO{-}CH{=}CH_2$	methyl vinyl ketone	Figure 1	Figure 4	Figure 8
70	$CH_2{=}C(OH)\text{-}CH{=}CH_2$	1,3-butadiene-2-ol	Figure 2	Figure 4	
98	C_6H_9OH	cyclohexen-1-ol	Figure 2	Figure 3	

PIMS of 1-butene heated in a pulsed He reactor (Figure S3 in the Supporting Information) shows extensive decomposition to methyl and allyl radicals around 1200 K; however, authentic samples of $CH_2{=}CH{-}CH{=}CH_2$ and cyclopentane are stable at 1200 K.

The product summary in Table 6 is gleaned from pyrolysis in two different microreactors. All of the PIMS and PIE spectra result from pyrolysis by a continuous reactor in a helium buffer gas, while the IR spectra utilize a pulsed microreactor with the cyclohexanone entrained in Ar. The operating conditions in these microreactors will be somewhat different. Simulations[12] of the fluid dynamics in the heated microreactors reveal that they are nonlinear devices. The chemistry varies exponentially with the temperature (which is rising) and quadratically with pressure (which is falling); consequently, most of the pyrolysis takes place in a small region near the middle of the reactor. The location and volume of this "sweet spot" in a pulsed Ar reactor will differ from that of a continuous He reactor. We therefore expect the initial decomposition temperature in a continuous flow He reactor (1200 K) will differ from that in a pulsed Ar reactor. All of the experiments indicate that temperatures at which both the isomerization/retro-Diels–Alder channel and radical fragmentation channels of Scheme 1 open are close to each other. In the future it might be possible to quantify[14] the ratio of products resulting from retro-Diels–Alder fragmentation to the radical products using ($CH_2{=}C(OH){-}CH{=}CH_2$) and (CH_2CHCH_2) as signatures of the respective pathways.

Problems of dissociative ionization can be better understood now. The essential factor driving the fragmentation of the radical cations [cyclohexanone]$^+$ and [methyl vinyl ketone]$^+$ is the isomerization of the ketones to the enols. Because the ionization energies of the enols, C_6H_9OH and $CH_2{=}C(OH){-}CH{=}CH_2$, are 1 eV below the that of the ketones (see Table 3), photoionization by 118.2 nm photons leads to the highly chemically activated ions, $[C_6H_9OH^*]^+$ and $[CH_2{=}C(OH){-}CH{=}CH_2{}^*]^+$. Photoionization of cyclohexanone with 118.2 nm (10.487 eV) light is 1.3 eV above threshold and Figure 1 displays no dissociative ionization. Heating $C_6H_{10}{=}O$ to 1200 K triggers isomerization to the enol, C_6H_9OH. Photoionization by 118.2 nm photons is 2.3 eV above the C_6H_9OH ionization threshold and dissociative ionization ensues. The fragmentation of $CH_3COCH{=}CH_2$ in Figure 5 can be explained the same way. At 300 K there is no dissociation of $CH_3COCH{=}CH_2{}^+$. Heating the sample to 1200 K isomerizes MVK to $CH_2{=}C(OH){-}CH{=}CH_2$ and lowers the ionization energy by 1 eV. Photoionization with 10 eV light is 0.4 eV above the *IE*(MVK) but is 1.4 eV over the ionization threshold of $CH_2{=}C(OH){-}CH{=}CH_2$.

Examination of the 118.2 nm cyclohexanone PIMS in Figure 1 shows the 300 K scan to be normal and only the parent ion[28,29] of cyclohexanone, *m/z* 98, and the ^{13}C-isotopomer (*m/z* 99) are observed. Appreciable cyclohexanone fragmentation is first observed upon heating to 1000 K when the enol, C_6H_9OH, is beginning to form. Both radical cations, $(C_6H_9OH)^+$ and $(CH_2{=}C(OH){-}CH{=}CH_2)^+$, would be expected to undergo a McLafferty rearrangement[31,32] and produce the chemically activated ketones, $[C_6H_{10}{=}O^*]^+$ and $[CH_3{-}CO{-}CH{=}CH_2{}^*]^+$. Possible pathways for dissociative ionization are shown in the Schemes S1 (cyclohexanone) and S2 (MVK), which are included in the Supporting Information.

There is one final complication that might affect the pyrolysis of cyclohexanone. The decomposition pathways in Scheme 2 show the three sets of diradicals (α, β, or γ) promptly extruding carbon monoxide or ketene. We should consider the consequences that would ensue if these radical pairs persisted long enough to react with each other. Recent shock tube studies[33] of the pyrolysis of cyclohexane in a shock tube reveal that around 1200–1300 K, *c*-C_6H_{12} isomerizes to $CH_2{=}CH{-}CH_2CH_2CH_2CH_3$. The six-membered ring ruptures a C–C bond and produces the diradical, $\bullet CH_2CH_2CH_2CH_2CH_2CH_2\bullet$, which persists long enough for an internal radical to abstract a hydrogen atom and produce the alkene, 1-hexene.

If the (α, β, or γ) radical pairs in Scheme 2 live long enough to disproportionate with each other, the chemistry in Scheme 5 results. The α radical pair could disproportionate to the aldehyde, $CH_2{=}CH{-}(CH_2)_3{-}CHO$, which is expected to decompose to the allyl radical (CH_2CHCH_2) and acrolein ($CH_2{=}CH{-}CHO$). Alternatively, the ketene ($CH_3CH_2CH_2CH_2CH{=}C{=}O$) could form and decompose to methyl radical (*m/z* 15) and the $CH_2CH_2CH_2CH{=}C{=}O$ radical, *m/z* 83. Disproportionation of the β radical pair yields the ketone, $CH_3CO{-}CH_2CH_2CH{=}CH_2$. Loss of allyl radical produces the CH_2COCH_3, which is expected to fragment to CH_3 and $CH_2{=}C{=}O$.

Disproportionation of the γ radical pair leads to the isomeric alkenes, $CH_3CH_2CH_2COCH{=}CH_2$ and $CH_2{=}CHCH_2COCH_2CH_2$. Both molecules are expected to dissociate

DOI: 10.1021/acs.jpca.5b10984
J. Phys. Chem. A 2015, 119, 12635–12647

Scheme 5. Products Arising from the Radical/Radical Disproportionation of the Three Sets of Radical Pairs Produced by Fragmentation of the Cyclohexanone Ring

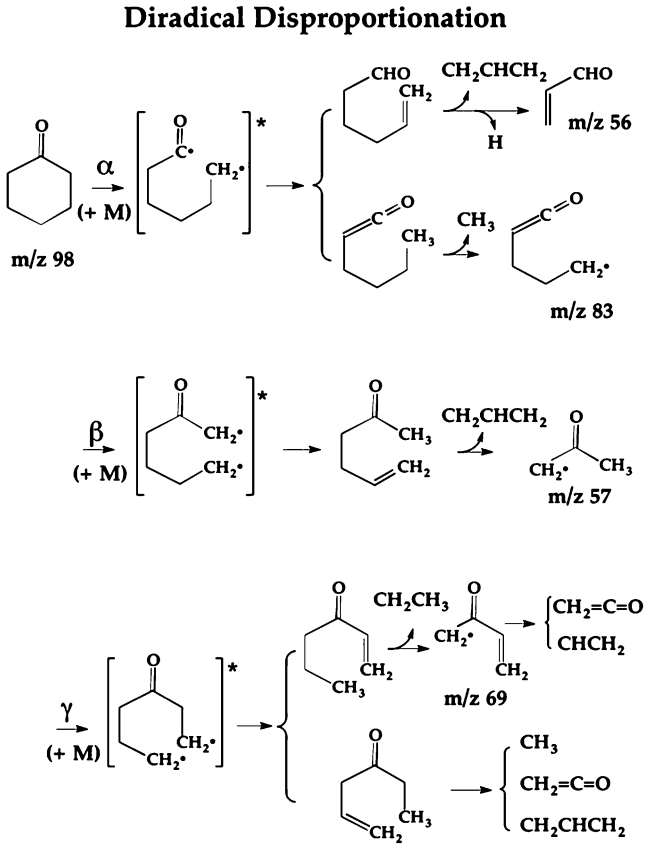

to a mixture of (CH_2CO, $CHCH_2$) and (CH_2CHCH_2, CH_2CO, CH_3).

There are few unique products arising from the radical/radical disproportionations of the (α, β, or γ) radical pairs. Weak signals from m/z 83 are present in Figure 1 at 1000 K that could be attributed to the $CH_2CH_2CH_2CH{=}C{=}O$ radical. It will be difficult to identify much of the chemistry in Scheme 5.

The results of cyclohexanone pyrolysis in a microreactor provide insight regarding the previous pyrolysis study.[3] It is important to remember that these two experiments have significant differences between them. The 1970 study carried out pyrolysis at 1300 K in a ceramic tube at low pressures (60 mTorr) with exposure times of approximately 10 ms. The decomposition products were collected and analyzed by electron impact mass spectroscopy and gas chromatography with a flame ionization detector; consequently, the identification of metastables and radical products is very difficult or simply impossible. Under these conditions,[3] the products of thermally cracking cyclohexanone were reported as listed in eq 1.

The results from this study are largely compatible with the 1970 results. The microreactor studies summarized in Table 6 include both ethylene and MVK, the two most important products from the ceramic flow reactor.[3] The origin of propene in eq 1 can plausibly be attributed to quenching of the CH_2CHCH_2 radicals. The radical channel in Scheme 2 is the pathway for formation of $CH_2{=}C{=}CH_2$, $CH_2{=}CHCH_2CH_3$, $CH_2{=}CH{-}CH{=}CH_2$, cyclopentane, and $CH_2{=}CH{-}CH_2{-}CH{=}CH_2$. Recombination of CH_3 radicals will produce the ethane in eq 1 and acetylene arises from the thermal cracking of MVK.

The cyclohexanone pyrolysis results in Table 6 are more difficult to compare to the recent $C_6H_{10}{=}O$ oxidation study of the jet-stirred reactor.[4] The conditions of the jet-stirred reactor (pressures of 10 atm, temperatures of 500−1200 K, and exposure times of 0.7 s) are significantly different from the microreactor studies here. The jet-stirred reactor examined the products of oxidation, while the present study is only that of anaerobic pyrolysis.

Some of the products from cyclohexanone pyrolysis in the microreactor in Table 6 agree with the predictions from the recent computational study.[5] This investigation examined the unimolecular thermal decomposition of cyclohexanone by the means of DFT electronic structure calculations and master equation simulations. Figure 2 in ref 5 explored several different pathways for cyclohexanone decomposition and predicted the keto/enol isomerization to cyclohexen-1-ol, followed by retro-Diels−Alder fragmentation.

The thermochemical estimates from the Introduction and a set of G3B3 calculations[5] suggest the lowest pathway for cyclohexanone pyrolysis to be the keto/enol isomerization, retro-Diels−Alder fragmentation, Scheme 1. At higher energies (roughly 0.5 eV) the radical channel pathways of Scheme 2 are predicted to appear; however, the experimental observations do not reveal distinct onsets of these two pathways. Both the PIMS spectra in Figures 2 and 5 and the IR spectrum (Figures 7 and 8) clearly reveal the presence of allyl radical and ketene (predicted from Scheme 2) as well as enols, C_6H_9OH and $CH_2{=}C(OH){-}CH{=}CH_2$ (predicted by Scheme 1), at 1200 K. The PIMS and IR spectra are consistent with simultaneous opening of the pathways in Schemes 1 and 2.

This study of the pyrolysis of cyclohexanone demonstrates the simplifying power of tunable synchrotron radiation as a VUV photoionization source. As the sample cyclohexanone is heated by the microreactor, isomerization of the ketone begins. The fixed frequency 118.2 nm PIMS spectrum in Figure 1 is cluttered with many ions that result from dissociative ionization of the target cyclohexanone, eq 3. The daughter ions from $[C_6H_9OH]^+$ fragmentation obscure many of the pyrolysis products. The problems with dissociative ionization could be circumvented by extensive use of matrix IR spectroscopy, and the effectiveness of a tunable VUV source offered by a synchrotron is evident from Figures 2−6. Experience from organic mass spectrometry predicts that ionization/fragmentation of cyclohexanone and, especially, its enol tautomer will not be an isolated case. Our experience with cyclohexanone here clearly demonstrates that use of tunable synchrotron VUV radiation is a solution to this problem.

■ ASSOCIATED CONTENT

Supporting Information

The Supporting Information is available free of charge on the ACS Publications website at DOI: 10.1021/acs.jpca.5b10984.

Description of the modified HEAT method, the pathways for dissociative ionization of cyclohexanone and MVK, and PIE curves for HCCH, CH_2CH_2, CH_3, and $CH_2CH{-}CHCH_2$ are presented as well as the PIMS for heated 1-butene, cyclopentane, and butadiene samples. (PDF)

DOI: 10.1021/acs.jpca.5b10984
J. Phys. Chem. A 2015, 119, 12635−12647

AUTHOR INFORMATION

Corresponding Author

*E-mail: barney@jila.colorado.edu.

Notes

The authors declare no competing financial interest.

ACKNOWLEDGMENTS

We acknowledge support from the National Science Foundation (CHE-1112466 and CBET-1403979) for J.P.P., J.H.B., G.T.B., J.W.D., and G.B.E. J.F.S. and T.L.N. also acknowledge support from the Robert A. Welch Foundation (Grant F-1283) and the United States Department of Energy, Basic Energy Sciences (DE-FG02-07ER15884). M.A., O.K., and T.P.T. and the Advanced Light Source are supported by the Director, Office of Energy Research, Office of Basic Energy Sciences, and Chemical Sciences Division of the U.S. Department of Energy under contract no. DE-AC02- 05CH11231. We are grateful to Dr. Aristotelis Zaras for extended discussions about the computational results for cyclohexanone pyrolysis. We are grateful for the helpful suggestions from the referees.

REFERENCES

(1) Boot, M.; Frijters, P.; Luijten, C.; Somers, B.; Baert, R.; Donkerbroek, A.; Klein-Douwel, R. J. H.; Dam, N. Cyclic Oxygenates: A New Class of Second-Generation Biofuels for Diesel Dngines. *Energy Fuels* **2009**, *23*, 1808−1817.

(2) Klein-Douwel, R. J. H.; Donkerbroek, A. J.; van Vliet, A. P.; Boot, M. D.; Somers, L. M. T.; Baert, R. S. G.; Dam, N. J.; ter Meulen, J. J. Soot and Chemiluminescence in Diesel Combustion of Bio-Derived, Oxygenated and Reference Fuels. *Proc. Combust. Inst.* **2009**, *32*, 2817−2825.

(3) De Mayo, P.; Verdun, D. L. Thermal Fragmentation of Cyclohexanone. *J. Am. Chem. Soc.* **1970**, *92*, 6079−6080.

(4) Serinyel, Z.; Togbé, C.; Zaras, A. M.; Dayma, G.; Dagaut, P. Kinetics of Oxidation of Cyclohexanone in a Jet-Stirred Reactor: Experimental and Modeling. *Proc. Combust. Inst.* **2015**, *35*, 507−514.

(5) Zaras, A. M.; Dagaut, P.; Serinyel, Z. Computational Kinetic Study for the Unimolecular Decomposition Pathways of Cyclohexanone. *J. Phys. Chem. A* **2015**, *119*, 7138−7144.

(6) Zhang, X. M.; Malick, D.; Petersson, G. A. Enolization Enthalpies for Aliphatic Carbonyl and Thiocarbonyl Compounds. *J. Org. Chem.* **1998**, *63*, 5314−5317.

(7) da Silva, G.; Kim, C.-H.; Bozzelli, J. W. Thermodynamic Properties (Enthalpy, Bond Energy, Entropy, and Heat Capacity) and Internal Rotor Potentials of Vinyl Alcohol, Methyl Vinyl Ether, and Their Corresponding Radicals. *J. Phys. Chem. A* **2006**, *110*, 7925−7934.

(8) Simmie, J. M.; Curran, H. J. Energy Barriers for the Addition of H, CH_3•, and •CH_2CH_3 to CH_2 = CHX X = H, CH_3, OH and for H-Atom Addition to RCH = O R = H, CH_3, •CH_2CH_3, n-C_3H_7: Implications for the Gas-Phase Chemistry of Enols. *J. Phys. Chem. A* **2009**, *113*, 7834−7845.

(9) Yang, X.; Yan, B.; Xu, H.-F.; Zhu, R.-H.; Zhang, M.-X.; Ding, D.-J. Analysis of Potential Energy Surface for Butanone Isomerization. *Chin. J. Chem. Phys.* **2013**, *26*, 519−525.

(10) Kiefer, J. H.; Shah, J. N. Unimolecular Dissociation of Cyclohexene at Extremely High-Temperatures - Behavior of the Energy-Transfer Collision Efficiency. *J. Phys. Chem.* **1987**, *91*, 3024−3030.

(11) Vasiliou, A.; Piech, K. M.; Zhang, X.; Nimlos, M. R.; Ahmed, M.; Golan, A.; Kostko, O.; Osborn, D. L.; Daily, J. W.; Stanton, J. F.; Ellison, G. B. The Products of the Thermal Decomposition of CH_3CHO. *J. Chem. Phys.* **2011**, *135*, 14306−14311.

(12) Guan, Q.; Urness, K. N.; Ormond, T. K.; David, D. E.; Ellison, G. B.; Daily, J. W. The Properties of a Micro-Reactor for the Study of the Unimolecular Decomposition of Large Molecules. *Int. Rev. Phys. Chem.* **2014**, *33*, 447−487.

(13) Ormond, T. K.; Scheer, A. M.; Nimlos, M. R.; Robichaud, D. J.; Daily, J. W.; Stanton, J. F.; Ellison, G. B. Polarized Matrix Infrared Spectra of Cyclopentadienone: Observations, Calculations, and Assignment for an Important Intermediate in Combustion and Biomass Pyrolysis. *J. Phys. Chem. A* **2014**, *118*, 708−718.

(14) Ormond, T. K.; Scheer, A. M.; Nimlos, M. R.; Robichaud, D. J.; Troy, T. P.; Ahmed, M.; Daily, J. W.; Nguyen, T. L.; Stanton, J. F.; Ellison, G. B. Pyrolysis of Cyclopentadienone: Mechanistic Insights From a Direct Measurement of Product Branching Ratios. *J. Phys. Chem. A* **2015**, *119*, 7222−7234.

(15) Vasiliou, A. K.; Kim, J. H.; Ormond, T. K.; Piech, K. M.; Urness, K. N.; Scheer, A. M.; Robichaud, D. J.; Mukarakate, C.; Nimlos, M. R.; Daily, J. W.; et al. Biomass Pyrolysis: Thermal Decomposition Mechanisms of Furfural and Benzaldehyde. *J. Chem. Phys.* **2013**, *139*, 104310−104321.

(16) Scheer, A. M.; Mukarakate, C.; Robichaud, D. J.; Nimlos, M. R.; Carstensen, H.-H.; Ellison, G. B. Unimolecular Thermal Decomposition of Phenol and d_5-Phenol: Direct Observation of Cyclopentadiene Formation via Cyclohexadienone. *J. Chem. Phys.* **2012**, *136*, 044309−044320.

(17) Prozument, K.; Park, G. B.; Shaver, R. G.; Vasiliou, A. K.; Oldham, J. M.; David, D. E.; Muenter, J. S.; Stanton, J. F.; Suits, A. G.; Ellison, G. B.; et al. Chirped-Pulse Millimeter-Wave Spectroscopy for Studies of Pyrolysis Reactions. *Phys. Chem. Chem. Phys.* **2014**, *16*, 15739−15751.

(18) Kidwell, N. M.; Vaquero-Vara, V.; Ormond, T. K.; Buckingham, G. T.; Zhang, D.; Mehta-Hurt, D. N.; McCaslin, L.; Nimlos, M. R.; Daily, J. W.; Dian, B. C.; et al. Chirped-Pulse Fourier Transform Microwave Spectroscopy Coupled with a Hyperthermal Reactor: Structural Determination of the Reactive Intermediate Cyclopentadienone. *J. Phys. Chem. Lett.* **2014**, *5*, 2201−2207.

(19) Urness, K. N.; Guan, Q.; Golan, A.; Daily, J. W.; Nimlos, M. R.; Stanton, J. F.; Ahmed, M.; Ellison, G. B. Pyrolysis of Furan in a Microreactor. *J. Chem. Phys.* **2013**, *139*, 124305−124314.

(20) Buckingham, G. T.; Ormond, T. K.; Porterfield, J. P.; Hemberger, P.; Kostko, O.; Ahmed, M.; Robichaud, D. J.; Nimlos, M. R.; Daily, J. W.; Ellison, G. B. The Thermal Decomposition of the Benzyl Radical in a Heated Micro-Reactor: I. Experimental Findings. *J. Chem. Phys.* **2015**, *142*, 044307−044320.

(21) Tajti, A.; Szalay, P. G.; Csaszar, A. G.; Kallay, M.; Gauss, J.; Valeev, E. F.; Flowers, B. A.; Vazquez, J.; Stanton, J. F. HEAT: High Accuracy Extrapolated *ab initio* Thermochemistry. *J. Chem. Phys.* **2004**, *121*, 11599−11613.

(22) Bomble, Y. J.; Vazquez, J.; Kallay, M.; Michauk, C.; Szalay, P. G.; Csaszar, A. G.; Gauss, J.; Stanton, J. F. High-Accuracy Extrapolated *ab initio* Thermochemistry. II. Minor Improvements to the Protocol and a Vital Simplification. *J. Chem. Phys.* **2006**, *125*, 064108−064116.

(23) Harding, M. E.; Vazquez, J.; Ruscic, B.; Wilson, A. K.; Gauss, J.; Stanton, J. F. High-Accuracy Extrapolated *ab initio* Thermochemistry. III. Additional Improvements and Overview. *J. Chem. Phys.* **2008**, *128*, 114111−114126.

(24) Nguyen, T. L.; McCarthy, M. C.; Stanton, J. F. Relatively Selective Production of the Simplest Criegee Intermediate in a CH_4/O_2 Electric Discharge: Kinetic Analysis of a Plausible Mechanism. *J. Phys. Chem. A* **2015**, *119*, 7197−7208.

(25) McQuarrie, D. A.; Simon, J. D. *Molecular Thermodynamics*; University Science Books: Sausalito, CA, 1999; p 450.

(26) *Vibration−Rotation Structure in Asymmetric- and Symmetric-Top Molecules*; Mills, I. M., Ed.; Academic Press: New York, 1972; Vol. *1*, pp 115−140.

(27) Nguyen, T. L.; Barker, J. R. Sums and Densities of Fully Coupled Anharmonic Vibrational States: A Comparison of Three Practical Methods. *J. Phys. Chem. A* **2010**, *114*, 3718−3730.

(28) Cocksey, B. J.; Eland, J. H. D.; Danby, C. J. Effect of Alkyl Substitution on Ionisation Potential. *J. Chem. Soc. B* **1971**, 790−794.

(29) Loudet, M.; Grimaud, M.; Metras, F.; Pfisterguillouzo, G. Intramolecular Interactions in Cyclohexane Series 0.2. Photoelectron-Spectra of 2-Chlorocyclohexanones. *J. Mol. Struct.* **1976**, *35*, 213−222.

(30) Shimanouchi, T. *Tables of Vibrational Frequencies, Consolidated*; NSRDS-NBS 39; Nat. Bur. Stand.: Washington, DC, 1972; Vol. *I*.

DOI: 10.1021/acs.jpca.5b10984
J. Phys. Chem. A 2015, 119, 12635−12647

(31) McLafferty, F. W.; McAdoo, D. J.; Smith, J. S.; Kornfeld, R. Enolic $C_3H_6O^{\bullet+}$ Ion Formed from Aliphatic Ketones. *J. Am. Chem. Soc.* **1971**, *93*, 3720−3730.
(32) McLafferty, F. W. *Interpretation of Mass Spectra*, 3rd ed.; University Science Books: Mill Valley, CA, 1980.
(33) Kiefer, J. H.; Gupte, K. S.; Harding, L. B.; Klippenstein, S. J. Shock Tube and Theory Investigation of Cyclohexane and 1-Hexene Decomposition. *J. Phys. Chem. A* **2009**, *113*, 13570−13583.
(34) Bartmess, J. E.; Scott, J. A.; McIver, R. T., Jr. The Gas Phase Acidity Scale from Methanol to Phenol. *J. Am. Chem. Soc.* **1979**, *101*, 6046−6056.
(35) Rienstra-Kiracofe, J. C.; Tschumper, G. S.; Schaefer, H. F., III; Nandi, S.; Ellison, G. B. Atomic and Molecular Electron Affinities: Photoelectron Experiments and Theoretical Computations. *Chem. Rev.* **2002**, *102*, 231−282.
(36) Pedley, J. B.; Naylor, R. D.; Kirby, S. P. *Thermochemistry of Organic Compounds*, 2nd ed.; Chapman and Hall: New York, 1986.
(37) Blanksby, S. J.; Ellison, G. B. Bond Dissociation Energies of Organic Molecules. *Acc. Chem. Res.* **2003**, *36*, 255−263.
(38) Moore, C. E. *Atomic Energy Levels*; NSRDS-NBS 35; Nat. Bur. Stand.: Washington, DC, 1971; Vol. *1*.
(39) Blush, J. A.; Chen, P.; Wiedmann, R. T.; White, M. G. Rotationally Resolved Threshold Photoelectron-Spectrum of the Methyl Madical. *J. Chem. Phys.* **1993**, *98*, 3557−3559.
(40) Pratt, S. T.; Dehmer, P. M.; Dehmer, J. L. Zero-Kinetic-Energy Photoelectron-Spectroscopy from the $\tilde{a}\ ^1A_u$ State of Acetylene - Renner-Teller Interactions in the *Trans*-Bending Vibration of $C_2H_2^+$ X $^2\prod_u$. *J. Chem. Phys.* **1993**, *99*, 6233−6244.
(41) Evans, M.; Ng, C. Y. Rotationally Resolved Pulsed Field Ionization Photoelectron Study of $CO^+(X\ ^2\sum^+, v^+ = 0-42)$ in the Energy Range of 13.98−21.92 eV. *J. Chem. Phys.* **1999**, *111*, 8879−8892.
(42) Willitsch, S.; Hollenstein, U.; Merkt, F. Ionization from a Double Bond: Rovibronic Photoionization Dynamics of Ethylene, Large Amplitude Torsional Motion and Vibronic Coupling in the Ground State of $C_2H_4^+$. *J. Chem. Phys.* **2004**, *120*, 1761−1774.
(43) Gao, H.; Xu, Y. T.; Yang, L.; Lam, C. S.; Wang, H. L.; Zhou, J. A.; Ng, C. Y. High-Resolution Threshold Photoelectron Study of the Propargyl Radical by the Vacuum Ultraviolet Laser Velocity-Map Imaging Method. *J. Chem. Phys.* **2011**, *135*, 224304−224311.
(44) Yang, Z. Z.; Wang, L. S.; Lee, Y. T.; Shirley, D. A.; Huang, S. Y.; Lester, W. A. Molecular-Beam Photoelectron-Spectroscopy of Allene. *Chem. Phys. Lett.* **1990**, *171*, 9−13.
(45) Xing, X.; Bahng, M. K.; Reed, B.; Lam, C. S.; Lau, K. C.; Ng, C. Y. Rovibrationally Selected and Resolved Pulsed Field Ionization-Photoelectron Study of Propyne: Ionization Energy and Spin-Orbit Interaction in Propyne Cation. *J. Chem. Phys.* **2008**, *128*, 094311−094315.
(46) Xing, X.; Reed, B.; Lau, K. C.; Ng, C. Y.; Zhang, X.; Ellison, G. B. Vacuum Ultraviolet Laser Pulsed Field Ionization-Photoelectron Study of Allyl Radical CH_2CHCH_2. *J. Chem. Phys.* **2007**, *126*, 171170−171174.
(47) Niu, B. H.; Bai, Y.; Shirley, D. A. High-Resolution Photoelectron-Spectroscopy and Femtosecond Intramolecular Dynamics of CH_2CO^+ and CD_2CO^+. *J. Chem. Phys.* **1993**, *99*, 2520−2532.
(48) Burrill, A. B.; Johnson, P. M. Torsional Analyses of *Trans*-2-Butene and Propene Pations: A Comparative Investigation of Two Prototypical Ions with Different Degrees of Symmetry. *J. Chem. Phys.* **2001**, *115*, 133−138.
(49) Zamanpour, M. H. N.; Bahkshandeh, A.; Ghaffarzadeh, S.; Dyke, J. M. Observation and Assignment of the First Photoelectron Band of the CH_3CO (X ^{2}A) Radical. *J. Electron Spectrosc. Relat. Phenom.* **2008**, *162*, 122−126.
(50) Knowles, D. J.; Nicholson, A. J. C. Ionization Energies of Formic and Acetic-Acid Monomers. *J. Chem. Phys.* **1974**, *60*, 1180−1181.
(51) Taatjes, C. A.; Hansen, N.; McIlroy, A.; Miller, J. A.; Senosiain, J. P.; Klippenstein, S. J.; Qi, F.; Sheng, L. S.; Zhang, Y. W.; Cool, T. A.; et al. Enols are Common Intermediates in Hydrocarbon Oxidation. *Science* **2005**, *308*, 1887−1889.
(52) Mallard, W. G.; Miller, J. H.; Smyth, K. C. The ns Rydberg Series of 1,3-*Trans*-Butadiene Observed Using Multiphoton Ionization. *J. Chem. Phys.* **1983**, *79*, 5900−5905.
(53) Bieri, G.; Burger, F.; Heilbronner, E.; Maier, J. P. Valence Ionization Energies of Hydrocarbons. *Helv. Chim. Acta* **1977**, *60*, 2213−2233.
(54) Masclet, P.; Mouvier, G. Study of Conjugated Ethylenic Aldehydes and Ketones Using Photo-Electric Spectrometry. *J. Electron Spectrosc. Relat. Phenom.* **1978**, *14*, 77−97.
(55) Turecek, F. 2-Hydroxybutadiene - Preparation, Ionization-Energy and Heat of Formation. *Tetrahedron Lett.* **1984**, *25*, 5133−5134.
(56) Krantz, A.; Goldfarb, T. D.; Lin, C. Y. Simple Method for Assigning Vibrational Frequencies to Rapidly Equilibrating Rotational Isomers. *J. Am. Chem. Soc.* **1972**, *94*, 4022−4024.
(57) Nandi, S.; Arnold, P. A.; Carpenter, B. K.; Nimlos, M. R.; Dayton, D. C.; Ellison, G. B. Polarized Infrared Absorption Spectra of Matrix-Isolated Allyl Radicals. *J. Phys. Chem. A* **2001**, *105*, 7514−7524.
(58) Moore, C. B.; Pimentel, G. C. Infrared Spectrum and Vibrational Potential Function of Ketene and Deuterated Ketenes. *J. Chem. Phys.* **1963**, *38*, 2816−2829.

DOI: 10.1021/acs.jpca.5b10984
J. Phys. Chem. A 2015, 119, 12635−12647